β-delayed fission of ^{180}Tl

J. Elseviers,[1] A. N. Andreyev,[2,3] M. Huyse,[1] P. Van Duppen,[1] S. Antalic,[4] A. Barzakh,[5] N. Bree,[1] T. E. Cocolios,[1,6]
V. F. Comas,[7] J. Diriken,[1] D. Fedorov,[5] V. N. Fedosseev,[8] S. Franchoo,[9] L. Ghys,[1] J. A. Heredia,[7] O. Ivanov,[1] U. Köster,[10]
B. A. Marsh,[8] K. Nishio,[3] R. D. Page,[11] N. Patronis,[1,12] M. D. Seliverstov,[1,6] I. Tsekhanovich,[13,14] P. Van den Bergh,[1]
J. Van De Walle,[6] M. Venhart,[1,15] S. Vermote,[16] M. Veselský,[15] and C. Wagemans[16]

[1]*Instituut voor Kern-en Stralingsfysica, KU Leuven, University of Leuven, B-3001 Leuven, Belgium*
[2]*Department of Physics, University of York, York, YO10 5DD, United Kingdom*
[3]*Advanced Science Research Center (ASRC), Japan Atomic Energy Agency (JAEA), Tokai-mura, Naka-gun, Ibaraki 319-1195, Japan*
[4]*Department of Nuclear Physics and Biophysics, Comenius University, 84248 Bratislava, Slovakia*
[5]*Petersburg Nuclear Physics Institute, 188350 Gatchina, Russia*
[6]*ISOLDE, CERN, CH-1211 Geneve 23, Switzerland*
[7]*Gesellschaft für Schwerionenforschung, Planckstrasse 1, D-64291 Darmstadt, Germany*
[8]*EN Department, CERN, CH-1211 Geneve 23, Switzerland*
[9]*Institut de Physique Nucléaire, IN2P3-CNRS/Université Paris-Sud, F-91406 Orsay Cedex, France*
[10]*Institut Laue Langevin, 6 rue Jules Horowitz, F-38042 Grenoble Cedex 9*
[11]*Department of Physics, Oliver Lodge Laboratory, University of Liverpool, Liverpool L69 7ZE, United Kingdom*
[12]*Department of Physics, University of Ioannina, GR-45110 Ioannina, Greece*
[13]*School of Physics and Astronomy, University of Manchester, Manchester M13 9PL, United Kingdom*
[14]*Centre d'Etudes Nucleaires de Bordeaux Gradignan, F-33175 Gradignan Cedex, France*
[15]*Slovak Academy of Sciences, Bratislava, SK-84511 Slovakia*
[16]*Department of Physics and Astronomy, University of Gent, Proeftuinstraat 86, B-9000 Gent, Belgium*

The detailed analysis of the β-delayed fission data of ^{180}Tl is presented. The experiment was performed by producing a pure beam of ^{180}Tl by means of highly selective resonance laser ionization followed by mass separation with the ISOLDE (CERN, Geneva) isotope separator. A surprising asymmetric mass distribution of fission fragments from ^{180}Hg, the daughter of ^{180}Tl β decays, was observed. Here, the energy calibration of the silicon detectors, which is crucial for a proper determination of the fission fragments' energy and mass split, is presented and the total kinetic energy and its dependence on the mass split ratio is discussed. A more precise β-delayed fission probability $P_{\beta DF}(^{180}\text{Tl}) = 3.2(2) \times 10^{-3}\%$ was deduced.

I. INTRODUCTION

Studies of low-energy fission, in which the excitation energy E^* of the fissioning nucleus is lower than or comparable to the height of its fission barrier B_f, represent a very important branch of fission studies. At these low excitation energies the influence of shell effects is especially important, while these effects are expected to wash out as the excitation energy of the nucleus is increased [1]. Furthermore, the relatively low (or even zero) angular momentum of the fissioning nucleus simplifies the analysis and the interpretation of experimental data in most cases.

Low-energy fission has been quite extensively studied in a broad mass region of the nuclear chart using different approaches: spontaneous fission from the ground state [2] and from shape isomers [3], fission induced by thermal neutrons [1,4], Coulomb-excited fission [5,6], and β-delayed fission (βDF) [7,8]. Using the observed fission fragment mass distributions, one can distinguish two broad and actually adjacent regions of nuclei in the nuclear chart. In particular, the nuclei in the light thorium to gold region, having a typical neutron-to-proton ratio of $N/Z \sim 1.4$–1.5, show a symmetric fission fragment distribution (*symmetric* fission), which was demonstrated, e.g., in the particle-induced fission

studies of $A \sim 200$ nuclei in Ref. [9,10] and more recently by the pioneering experiments using Coulomb-excited fission of relativistic radioactive beams [5,6]. In contrast to this, fission of nuclei in the heavier actinides region, having a typical ratio of $N/Z \sim 1.55$, results in most cases in an asymmetric mass distribution of the fission fragments (*asymmetric* fission), as, e.g., in the thermal neutron-induced fission of ^{235}U or in the majority of known cases of spontaneous fission [1,2]. An elegant method of low-energy fission studies in this region is βDF [7,8], which was recently applied for, e.g., neutron-deficient isotopes ^{242,244}Es and ^{238}Bk to study the mass distribution of their respective daughter (after β decay) isotopes ^{242,244}Cf [11,12] and ^{238}Cm [13].

In the βDF process, discovered in 1966 [7], the parent nucleus first undergoes β decay (β⁻ or β⁺/EC), whereby it populates an excited state in the daughter nucleus. If this excited state has an energy comparable to or higher than the fission barrier of the daughter nucleus, it may fission with a finite probability. This decay mode will happen in competition with γ and/or particle (neutron or proton) decay. So far, this process was observed in only a dozen of very neutron-deficient nuclei in the transuranium region [8] and a few nuclei in the lead region [14–17], and in the neutron-rich region several cases of βDF are known [18]. The most recent review of βDF

is given in Ref. [18]. In the heavy neutron-deficient nuclei, and especially when the β decay populates high-lying levels close to and above the fission barrier, electron capture (EC) decay typically dominates over β^+ decay. Therefore, in the literature this decay is often called EC-delayed fission (ECDF).

The maximum excitation energy of the daughter nucleus in this process is determined by the β-decay Q value, Q_{EC}, of the parent nucleus, which typically does not exceed 5–6 MeV in the uranium region and 11–12 MeV in the most neutron-deficient nuclei in the lead region. These values can be compared to the typical (*calculated*) values of the fission barriers in the respective regions, which are 3–7 MeV in the uranium nuclei of interest and 9–12 MeV in the lead region (see Table V of Ref. [19]). At this point we have to note that experimental masses (thus Q_{EC} values) and fission barriers are not available for these exotic nuclei. Values quoted throughout this paper are taken from the theoretical work by Möller *et al.* in Ref. [19]. The choice of theoretical model has negligible impact on the conclusions of this work.

Owing to relatively low Q_{EC} values, the βDF can be classified as low-energy fission. Furthermore, the comparison of the above Q_{EC} and B_f values shows that fission in most known βDF cases is subbarrier, meaning that it proceeds from excited states below the fission barrier ($Q_{EC} - B_f \leqslant 0$). Additionally, βDF allows low-energy fission studies of nuclei with very exotic N/Z ratios, which do not fission from their ground state, owing to their relatively high fission barrier.

Recently, we initiated an extensive campaign of βDF studies of nuclei in the neutron-deficient lead region, possessing a typical ratio of $N/Z = 1.25$–1.3, opening a new region in low-energy fission [16,17].

In particular, in our βDF study of ^{180}Tl [15] the fission fragments mass distribution from the fission of its daughter (after β decay) isotope ^{180}Hg ($N = 100$, $Z = 80$, $N/Z = 1.25$) was measured for the first time. Before that study, symmetric fission of ^{180}Hg into two semimagic nuclei ^{90}Zr ($N = 50$, $Z = 40$) was expected. In contrast to this, a surprising asymmetric mass split in nuclei in the vicinity of $A \approx 80$ and $A \approx 100$ was observed in Ref. [15]. This finding was discussed within the five-dimensional fission model developed by Möller *et al.* [19]. Following this discussion, the fission of even-A isotopes of mercury was analyzed within the Brownian Metropolis shape-motion treatment [20]. Further, the self-consistent nuclear density functional theory employing Skyrme SKM* and Gogny DIS energy density functionals was used to study the fission of ^{180}Hg and ^{198}Hg [21]. Two further approaches were inspired by the earlier scission-point model [22]. The authors of Ref. [23] use what they call the "improved scission-point" model and in Ref. [24] the recently developed microscopic scission-point model is used, whereby the individual potential of each fragment is derived in the framework of Hartree-Fock-Bogoliubov microscopic calculations with the Gogny effective nucleon-nucleon force.

This experiment was performed at the on-line isotope separator ISOLDE (CERN, Geneva) [25] and was part of a systematic α, β, and β-delayed fission study of a series of neutron-deficient thallium isotopes $^{178-182}$Tl. A dedicated β-decay study of ^{180}Tl has been described in our recent paper [26] and we concentrate here on the βDF results only.

The present paper provides experimental details and improved analysis of the data reported in Ref. [15]. The βDF study of ^{178}Tl, resulting from the same set of experiments, is reported in the accompanying paper [27].

The structure of the paper is as follows. Section II gives the description of the experimental setup and measurement procedure, followed by the energy calibration of the silicon detectors in Sec. III. The obtained results, including the energy and mass distributions, are then discussed in Sec. IV.

II. EXPERIMENTAL SETUP

The thallium isotopes of interest were produced by proton-induced spallation reactions of a thick uranium target at ISOLDE. The proton beam from the PS booster of CERN, having an energy of 1.4 GeV and an average intensity of 2.1 μA, impinged on a 50 g/cm^2 UC$_x$ target, producing a wide variety of radioactive nuclei. The proton beam consisted of 2.4-μs proton bunches that had a period of 1.2 s or a multiple of 1.2 s. A sequence of 21 pulses was logically grouped into a so-called *supercycle* with a total length of 25.2 s. The number of proton pulses that ISOLDE received per supercycle was changed from four to ten pulses throughout the experiment, depending on the specific requirements, as discussed further.

After production, the recoiling nuclei were stopped in the target material. The radioactive nuclei diffused out of the target matrix and effused towards the hot cavity where resonant laser ionization took place. To reduce the release time, the target-ion source was kept at a high temperature of $\approx$2300 K. In the Resonance Ionization Laser Ion Source (RILIS) [28] the desired thallium isotopes were resonantly excited from the atomic ground state to an intermediate electronic state by a frequency-doubled laser beam at 276.79 nm and subsequently ionized to a 1$^+$ charge state by a powerful 532.5-nm beam of a 10-kHz pulsed Nd:YAG laser. The produced ions were extracted from RILIS, accelerated by a 30-keV electric field and separated according to their mass-to-charge ratio with the magnetic dipoles of the High Resolution Separator (HRS) of ISOLDE [29]. As a result of selective ionization with RILIS and subsequent mass analysis with HRS, a high-purity beam of ^{180}Tl nuclei was obtained.

To detect the radioactive decay of the ^{180}Tl nuclei, the Leuven windmill system was used; see Fig. 1. After mass
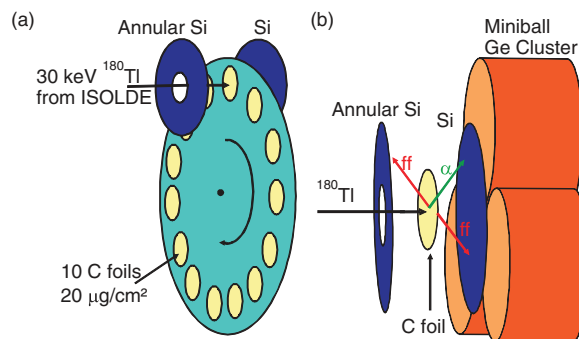

FIG. 1. (Color online) A schematic view of the windmill system is shown in (a) and a magnification of the detector arrangement is shown in (b) [15].

separation, the incident 30-keV Tl$^+$ ion beam of $\sim$150 atoms/s was implanted in a 20 μg/cm^2 thick carbon foil. Ten of these carbon foils were mounted on a rotating wheel. The longer-living daughter products of ^{180}Tl were removed from the implantation position by rotating the wheel after each supercycle, which introduced the next foil to the implantation position. The time structure of the measurement is described in details in Fig. 2 of Ref. [26] and only the most relevant features are provided here. The time structure of the measurement was determined by the half-life of ^{180}Tl, which was known from literature to be 1.5(2) s [30]. Therefore, the proton pulses were chosen in such a way that two consecutive proton pulses with 1.2 s time between them were taken followed by a period without proton pulses. The opening of the separator gate, which allows the radioactive ions to pass towards the detection system, was synchronized with the proton pulse structure and was opened from the moment the first proton pulse arrived until 1.2 s after the second proton pulse (i.e., 2.4 s), after which the separator gate closed. Thus, during the first 2.4 s of the measurement, continuous implantation data were measured, followed by a period of pure decay; see Fig. 2 of Ref. [26]. Different groups of such two consecutive pulses were chosen during the experiment, depending on the specific type of measurements (α decay, β decay, βDF, or half-life).

Two silicon detectors were placed in close geometry at the implantation position, as shown in Fig. 1. An annular detector having an active area of 450 mm^2, thickness of 300 μm, and a central hole with a diameter of 6 mm (Ortec Surface Barrier detector [31]) was positioned at a distance of $\sim$7 mm upstream of the foil, so that the ion beam was passing through this hole before being implanted into the foil. A circular detector of active area 300 mm^2 and thickness 300 μm (Canberra PIPS detector [32]) was placed $\sim$4 mm downstream of the foil. The use of two silicon detectors increases the geometrical efficiency and allows the measurement of double-fold fission fragments in coincidence. The total detection efficiency for an α particle or single fission fragment in any of the Si detectors was about 51%, while coincident fission fragments were registered with an efficiency of about 16%. These values are slightly lower than 66% and 20% given in our first paper [15]; this is attributable to a better estimation of the geometry of the setup and relative positions between the foils and silicon detectors, made using GEANT4 simulations [33]. Note that this does not influence the determination of the βDF probability because it is normalized to the number of detected fission fragments and α's detected in the same detector (see Sec. IV C). Because the primary aim of this experiment was the detection of βDF, the energy range of the silicon-detector electronics was set to 200 keV–100 MeV to record events from electrons, positrons, α particles, and fission fragments. The measured energy resolution [full width at half maximum (FWHM)] for α decays in the range of 5000–7000 keV was $\sim$35 keV, which was mostly determined by the electronics owing to the necessity to cover a large energy range.

A Miniball germanium cluster detector, which consisted of three hyperpure germanium (HPGe) crystals [34] and a planar germanium detector of the "low-energy germanium (LeGe)" type [35] were placed in close geometry outside the vacuum chamber, to allow γ and K x-ray measurements in coincidence

with α and β particles and fission fragments. The typical energy resolution (FWHM) of each crystal of the cluster and the LeGe detector for 1.3 MeV radiation was $\sim$3.1 keV. The analog signals from the preamplifiers were digitized using digital electronics (DGF-4C modules [36]) and for every decay event, the energy and time were recorded in the data system. One of the advantages of these DGF modules is that the data can be stored in 64k channels, allowing a good resolution for the large energy range that should be covered.

III. ENERGY CALIBRATION PROCEDURE FOR SILICON DETECTORS

As a first step in the data analysis, a proper energy calibration of the silicon detectors in the fission fragment energy range of $\sim$40–100 MeV had to be performed. This calibration, however, is not straightforward, because semiconductor detectors suffer from what is known as the pulse height defect (PHD). Owing to this effect, the total charge, which is proportional to the pulse height (PH), collected in the detector for a heavy ion is usually smaller than that of an α particle or a light ion for the same energy deposition inside the active volume of the silicon detector. Therefore, the measured PH is no longer strictly proportional to the energy of the incoming heavy ion, but will also depend on its mass [37,38]. The PHD is attributable to physical processes occurring in the detector's material, one of the most important being the increased recombination of charge carriers for the heavier ions, as they produce a denser ionization track in the silicon detector [39,40].

The importance of a proper account for the PHD effect for fission fragments with typical energies in the range of 30–120 MeV and masses of 40–150 amu is well known, particularly in the experiments using silicon detectors. Specifically in the case of asymmetric fission, it is imperative to accurately account for different PHDs for the light and heavy masses. In the past, a special procedure to calibrate silicon detectors for such measurements was developed and by now became a well-accepted method [37,38].

For an incoming ion of a given mass, a linear relationship between PH x and energy E remains,

$$E = C_1 x + C_2, \tag{1}$$

where C_1 and C_2 are constants. However, the PHD leads to a mass dependence of the coefficients C_1 and C_2. To study this effect, in their original work, Schmitt *et al.* [37] investigated the response of silicon detectors to ^{79,81}Br and ^{127}I ions that were accelerated in a Van de Graaff accelerator. Data were taken in the energy range between 30 and 120 MeV. They found that C_1 and C_2 are approximately linearly dependent on the ion mass,

$$E = (a + a'm)x + b + b'm, \tag{2}$$

where m is the mass of the incoming ion and a, a', b, and b' are constants for a particular detector. Schmitt *et al.* [37] established a link between these constants and the mean PHs of the light and heavy fragment groups of a reference fissioning isotope, e.g., ^{252}Cf, through universal constants for that specific fissioning isotope. Later these constants were improved by

Weisenberger *et al.* [38]. However, these constants are not used in the current calibration, as the authors of Ref. [38] already pointed out that their constants are deduced for one specific type of detector (i.e., ORTEC [31] F series, active area 100 mm^2). It is not sure that they can also be used for other types of silicon detectors. Therefore, a new calibration measurement was performed at the Lohengrin spectrometer of the Institut Laue-Langevin (ILL) in Grenoble. Fission fragments resulting from the ^{235}U(n, f) reaction can be separated according to their mass-to-charge A/q and energy-to-charge E/q ratio by two dipole bending magnets. Our silicon detector was placed behind the Lohengrin spectrometer on a rotating holder such that it was possible to also measure the fission fragments at a certain angle with respect to the beam axis. Further, a ^{241}Am source was used as a reference source and was mounted at the backside of the detector. Without breaking the vacuum, the detector could then be rotated over 180° to either face the ^{241}Am source or the fission fragment beam direction. As such, the masses and energies of the fission fragments were measured for all except one of the used detectors in the current experiment. The one detector that was not recalibrated, did not work anymore at the time of measurement at ILL. Another detector of the same type was calibrated and possible differences in the calibration are taken into account in the systematic error discussed below.

From these measurements, it was possible to deduce an α calibration relation of the form Eq. (1) and a calibration for the fission fragments using Eq. (2). By assuming that the offset [b and b' in Eq. (2)] remains constant and by taking the ratio of the gain of the fission calibration [a and a' in Eq. (2)] to that of the α calibration ($c = a/C_1$ and $c' = a'/C_1$), new constants for a specific detector can be deduced, namely c, c', b, and b'. To calibrate the same detector in a new experiment, only the α calibration needs to be known. This α calibration can be scaled to the constants for that detector, by multiplying the gain of this calibration with c and c' to get the parameters a and a' in Eq. (2), while b and b' remain constant. Specific details on how this calibration procedure was developed are not discussed here, but will be reported in Ref. [41]. The deduced calibration constants for the current experiment are

$$
\begin{aligned}
a_1 &= 1.814(18) \times 10^{-3} & a_2 &= 1.707(17) \times 10^{-3}, \\
a_1' &= 1.8946(2) \times 10^{-6} & a_2' &= 2.4191(2) \times 10^{-6}, \\
b_1 &= -0.57(43) & b_2 &= 0.94(51), \\
b_1' &= 3.57(44) \times 10^{-2} & b_2' &= 2.23(52) \times 10^{-2}.
\end{aligned} \tag{3}
$$

The index 1 is used for the annular detector (referred to as detector 1); 2 is used for the detector downstream of the foil (detector 2). These constants also have a systematic error, which follows primarily from the fact that the constants, determined for one specific detector, were deduced from the ^{235}U(n, f) reaction. The fission fragments resulting from this reaction have a different N/Z ratio in comparison with the fission fragments from the βDF of ^{180}Tl. In, for example, Refs. [42–44], they all assume a strong influence on the PHD of the stopping power or thus the energy loss in a detector. Because, according to the Bethe-Bloch equation, the energy loss in a detector depends primarily on the velocity and effective charge of the ions, in addition to the mass and
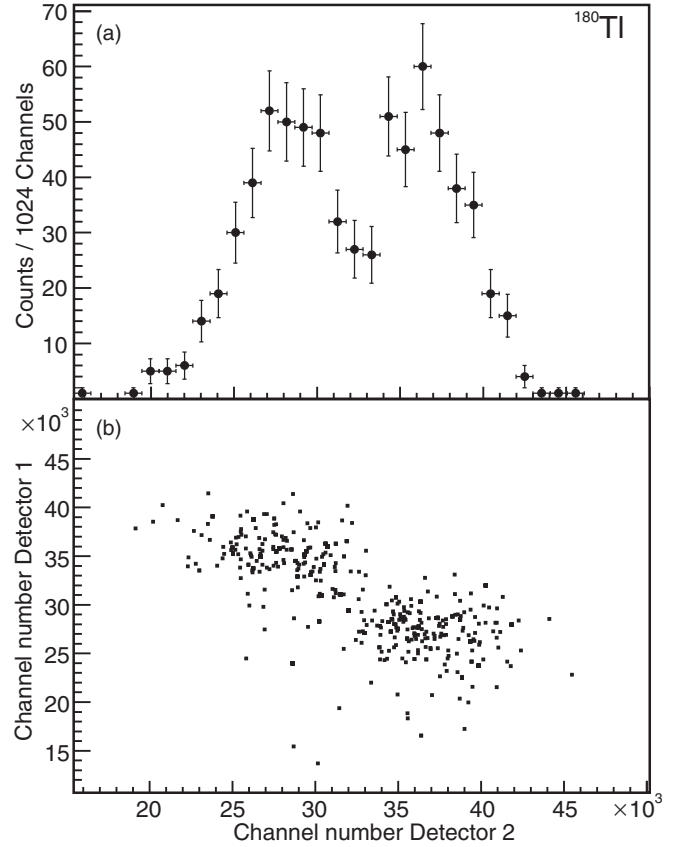

FIG. 2. (a) Uncalibrated energy spectrum of single fission events in the βDF of ^{180}Tl in detector 2. (b) Uncalibrated energy spectrum of coincident fission events in the βDF of ^{180}Tl (344 in total). Detector 1 is the annular detector located upstream and detector 2 is the one downstream of the carbon foil.

energy, which are taken into account in Eq. (2), it is plausible that different N/Z values would also correspond to different calibration constants. To estimate the systematic error on the calibration constants, the PHDs of different isotopes measured at ILL were compared. From this comparison it is clear that the PHD increases with about 1 MeV when increasing simultaneously the mass A with ten units and the charge Z with four units. This is true for the mass range that covers the fragment distribution from the βDF of ^{180}Tl. In the βDF of ^{180}Tl, the most probable isotopes are ^{80}Kr ($Z = 36$) and ^{100}Ru ($Z = 44$) (see Sec. IV A). In the ^{235}U(n, f) reaction the most probable isotopes for the masses $A = 80$, 90, and 100 are (see, e.g., [45]) ^{80}Ge ($Z = 32$), ^{90}Kr ($Z = 36$), and ^{100}Zr ($Z = 40$). One notices that for the same mass A, the charge Z is always higher in the case of the fission fragments from the βDF of ^{180}Tl. It is clear that for, e.g., ^{80}Kr the PHD should lie between the PHDs of ^{80}Ge and ^{90}Kr. Therefore, the calibrated energy of ^{80}Kr should be shifted with 0.5 MeV with a systematic error of 0.5 MeV. This argumentation holds for every fragment detected in the βDF of ^{180}Tl.

Figure 2 shows the PH (uncalibrated) spectra obtained in the case of the βDF decay of ^{180}Tl. This figure alone clearly demonstrates the asymmetric mass split of ^{180}Hg. Equation (2)

along with the momentum and mass conservation laws can now be used to calibrate the fission spectra of ^{180}Hg according to this set of expressions:

$$E_1 = (a_1 + a'_1 m_1)x_1 + b_1 + b'_1 m_1,$$
$$E_2 = (a_2 + a'_2 m_2)x_2 + b_2 + b'_2 m_2, \qquad (4)$$
$$m_1^\star E_1^\star = m_2^\star E_2^\star, \quad m_1^\star + m_2^\star = A_f = 180.$$

Here, x_i are the *measured* PHs of the fission fragments in the detector i ($i = 1, 2$) (see Fig. 2), while E_i and m_i are their resulting energies and masses, which we aim to deduce. If neutron emission occurs in the fission process, E_i and m_i are the quantities after neutron emission (*post*neutron quantities). $E_i^\star$ and $m_i^\star$ are the corresponding initial quantities, before neutron emission during fission, thus the *pre*neutron quantities [46], and $A_f = 180$ is the mass number of the fissioning ^{180}Hg nucleus. By using this calibration procedure it is only possible to calibrate coincident fission events, because the measured PH of both fission fragments will have to be inserted simultaneously in the above equations.

We use $A_f = 180$ because the neutron separation energy $S_n(^{180}\text{Hg}) = 11\,390(30)$ keV [47] is above the $Q_{EC}(^{180}\text{Tl}) = 10\,840(120)$ keV [47], thus preventing neutron emission from ^{180}Hg after the β decay of ^{180}Tl. The proton separation energy is $S_p(^{180}\text{Hg}) = 2582(22)$ keV [47], but, owing to the Coulomb barrier, the β-delayed proton emission probability is very small. Further, HgK x rays in coincidence with fission fragments were observed and a half-life of ^{180}Tl was deduced from the βDF branch that is in agreement with the half-life determined from the α- and β-delayed γ decay branch (see further in the text, Fig. 7 and Sec. IV B).

To solve this system of equations the quantities E_i and $E_i^\star$ and m_i and $m_i^\star$ have to be related. This can be done by taking into account the number of neutrons emitted in the fission ν_i, the corresponding energy carried away by the neutrons $\Delta E_{i,\nu}$, and the energy loss of the fission fragment owing to their interaction with matter during their flight from the source to the active volume of the silicon detector $\Delta E_{i,\text{int}} = \Delta E_{i,\text{cf}} + \Delta E_{i,\text{dl}}$. The latter contribution consists of the energy loss of the fragment in the implantation carbon foil $\Delta E_{i,\text{cf}}$ and in the dead layer of the detector $\Delta E_{i,\text{dl}}$ (which will increase when the fragments are detected at a certain angle). These considerations lead to the following relations:

$$E_i^\star = E_i + \Delta E_{i,\nu} + \Delta E_{i,\text{int}}$$
$$= E_i + \Delta E_{i,\nu} + \Delta E_{i,\text{cf}} + \Delta E_{i,\text{dl}}, \qquad (5)$$
$$m_i^\star = m_i + \nu_i.$$

In the determination of the calibration parameters, the $\Delta E_{i,\text{dl}}$ term is already taken into account in the constants a through b' if the fragments are detected under the same angle. However, our calibration constants were determined for perpendicular impingement, while the fragments in the βDF of ^{180}Tl were detected at a certain angle. Also, the $\Delta E_{i,\text{cf}}$ cannot simply be neglected because the fission fragments from which the calibration parameters were deduced did not need to penetrate the carbon foil.

In the literature, to estimate the energy loss caused by the emitted neutrons $\Delta E_{i,\nu}$ in the fission of transuranium nuclei, a

procedure introduced by Balagna *et al.* [48], is used, see, e.g., Fig. 8 in Ref. [49]. This procedure relies on the knowledge of the average number of neutrons emitted as a function of fragment mass, $\tilde{\nu}(M)$, which was measured for, e.g., ^{257}Fm in Ref. [48] and which showed a staggering behavior in the range of $\tilde{\nu} \sim 1$–4. As no such data exist for the very neutron-deficient nuclei in the lead region, we used a simplified estimate, as described below. However, anticipating the discussion below, we mention that based on our analysis we concluded that most probably only one neutron could be emitted in the fission of ^{180}Hg. The corresponding correction of the mass distributions owing to the neutron emission should thus be much less than in the uranium region, where values up to $\tilde{\nu} \sim 4$ are observed.

In our case, to estimate the energy loss caused by the emitted neutrons $\Delta E_{i,\nu}$, we use the generally accepted assumption that the neutrons are emitted after the fission fragments have reached their maximum velocity $v_i^\star$. Second, it is assumed that the average velocity of the fission fragments is not changed by the emission of neutrons, because the neutrons will be emitted isotropically in the center of mass (the velocity distribution, however, will be broadened). These two assumptions are supported experimentally [1]. The average energy of the fragments after neutron emission can then be estimated by (neglecting the recoil energy [46])

$$\bar{E}_i \approx \frac{1}{2}m_i v_i^2 = \frac{1}{2}m_i v_i^{\star 2} = \frac{m_i}{m_i^\star}E_i^\star. \qquad (6)$$

With this expression $\Delta E_{i,\nu}$ is given by

$$\Delta E_{i,\nu} = E_i^\star - E_i = \frac{\nu_i}{m_i^\star}E_i^\star. \qquad (7)$$

This gives the following set of equations, which have to be solved iteratively (with $F_i = 1 - \nu_i/m_i^\star$),

$$E_i^\star = (a_i/F_i + a'_i m_i^\star)x_i + b_i/F_i + b'_i m_i^\star$$
$$+ \Delta E_{i,cf}/F_i + \Delta E_{i,dl}/F_i, \qquad (8)$$
$$m_1^\star E_1^\star = m_2^\star E_2^\star, \quad m_1^\star + m_2^\star = A_f.$$

In a first approximation F_i will be set equal to one by setting the number of emitted neutrons ν_i to zero. In Sec. IV A we return to this issue. The system of equations Eq. (8) can now be solved with respect to $m_1^\star = m_1$ (when $F_i = 1$ or $\nu_i = 0$). It follows that $m_1^\star$ must be the solution of a quadratic equation,

$$Am_1^{\star 2} + Bm_1^\star + C = 0, \qquad (9)$$

with

$$A = a'_1 x_1 + b'_1 - a'_2 x_2 - b'_2,$$
$$B = a_1 x_1 + b_1 + a_2 x_2 + b_2 + 2A_f a'_2 x_2 + 2A_f b'_2$$
$$+ \Delta E_{i,cf} + \Delta E_{i,dl},$$
$$C = -A_f(a_2 x_2 + a'_2 A_f x_2 + b_2 + A_f b'_2).$$

To solve this equation the energy loss in the carbon foil and the shift in energy necessary to account for the detection of fission fragments at a certain angle has to be known. These energy shifts, however, can only be estimated.

To determine the mean energy loss of the fission fragments in the carbon foil the program TRIM was used [50]. First, the

distribution of the depth of implantation of the 30-keV ^{180}Tl beam was determined. This resulted in a mean implantation depth of $d \approx 180$ Å, corresponding to the first one-fifth part of the foil. This means that the fragments flying towards detector 1 will lose less energy than those flying towards detector 2. The distribution of the implantation depth was then used as an input to start the energy loss calculations for the fission fragments. A TRIM simulation was performed for a range of isotopes with a different energy and mass. It was assumed that the fragments are randomly emitted in 4π. In addition, a beam spot size of 6 mm diameter with uniform density was included in the simulations. Finally, the size of the detectors (including the central hole in detector 1) was also taken into account. This resulted in a mean energy loss of 0.3(1) MeV for the fragments flying towards detector 1 and an energy loss of 1.2(3) MeV for the fragments flying to detector 2 (more details can be found in Refs. [51,52]). This energy loss was therefore taken into account by assuming that every fragment flying in direction of detector 2 loses 1.2 MeV and every fragment flying to detector 1 loses 0.3 MeV. This is only an estimation, which will slightly depend on the angle of emission and mass/atomic number of the fission fragments.

To estimate the energy shift necessary to take into account the fact that the fission fragments are measured at a certain angle and do not impinge perpendicular on the detector, a dedicated measurement where the fission fragments were detected at an angle of 45° was performed during the ILL campaign. This angle is very close to the mean angle of impingement of about 43°. This measurement showed that the measured energy is smaller by about 0.3 MeV for detector 1 and about 1.0 MeV for detector 2 when the fission fragments reach the detector at an angle of 45°. However, this shift is also only an estimation, because the fission fragments reach the detectors at different angles. Therefore, the systematic error on these shifts was taken as large as the shift itself.

With these energy shifts taken into account, Eq. (9) can be solved and gives the mass of the fragments detected in detector 1. The energy can further be deduced from Eq. (2). The mass of the fragments detected in detector 2 can be obtained by exchanging the labels 1 and 2 in the above equation or simply from $m_2^\star = A_f - m_1^\star$.

As mentioned above, the used calibration procedure entails some systematic errors:(i) errors on the deduced calibration constants are attributable to the different N/Z values; (ii)the fission fragments do not impinge the detector perpendicular but at a certain angle, while the calibration constants were deduced for perpendicular impingement; (iii) the energy loss in the carbon foil is not a constant, but varies according to the emission angle. These different energy shifts together with their systematic errors are summarized in Table I. The total systematic error of the two detectors and of the total kinetic energy (TKE) (see Sec. IV A) is also given. In the remainder of this article these total systematic errors are always added to the statistical error of the quoted energies.

By using the procedures described in this section, we obtained the energy calibrated and the mass spectra for fission fragments, which are discussed in the next section.

TABLE I. The different energy shifts and their systematic errors that need to be taken into account to determine the TKE are given. More details are given in the text.

Description	Shift and systematic error (MeV)
(i) N/Z-value detector 1	0.5(5)
(i) N/Z-value detector 2	0.5(5)
(ii) Angle detector 1	0.3(3)
(ii) Angle detector 2	1.0(10)
(iii) Carbon foil detector 1	0.3(1)
(iii) Carbon foil detector 2	1.2(3)
Total systematic errors	
Energy in detector 1	0.6
Energy in detector 2	1.2
TKE	1.3

IV. EXPERIMENTAL RESULTS AND DISCUSSION

A. Energy and mass distributions resulting from the fission of ^{180}Hg

The mass spectrum for 344 coincident events is shown in Fig. 3. The figure shows a mirror plane at $A = 180/2 = 90$, owing to the condition $m_2^\star = A_f - m_1^\star$. The result of the Gaussian fit gives $A_L = 80(1)$ amu for the light and $A_H = 100(1)$ amu for the heavy fragment with a full width at half maximum (FWHM) of 10.9(5) amu for the mass distribution. From the data of the current experiment, it is not possible to deduce the Z value of the fission fragments. Therefore, the most probable Z values of the heavy and light fission fragments were deduced to be $Z_H = 44(2)$ and $Z_L = 36(2)$, respectively, by assuming that the $N/Z = 1.25$ ratio of the parent nucleus ^{180}Hg is approximately preserved in the fission fragments. This is a generally accepted approach in fission studies, but remains a simplification. Probably a wide range in Z values is present among the fission fragments. Further, as the fissioning nucleus is an even-even nucleus, it is expected that the fission fragments will also be even-even nuclei, if no neutrons are emitted. These considerations lead to fission fragments in the vicinity of ^{80}Kr, which has $N/Z = 1.22$ and of ^{100}Ru, $N/Z = 1.27$, which are
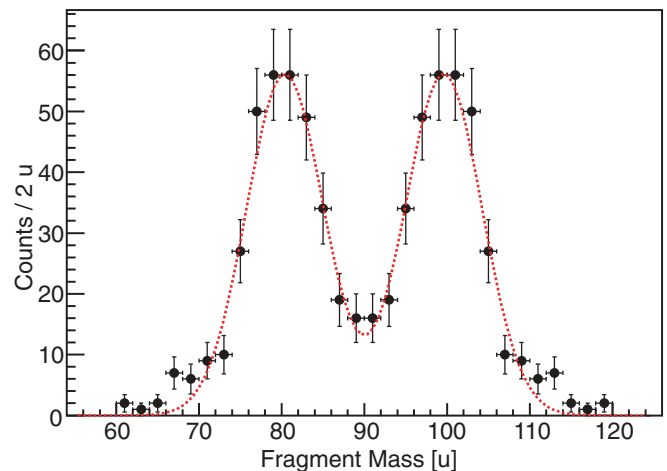

FIG. 3. (Color online) Mass distribution of the fission fragments. The red dotted line shows the Gaussian fit through the data.
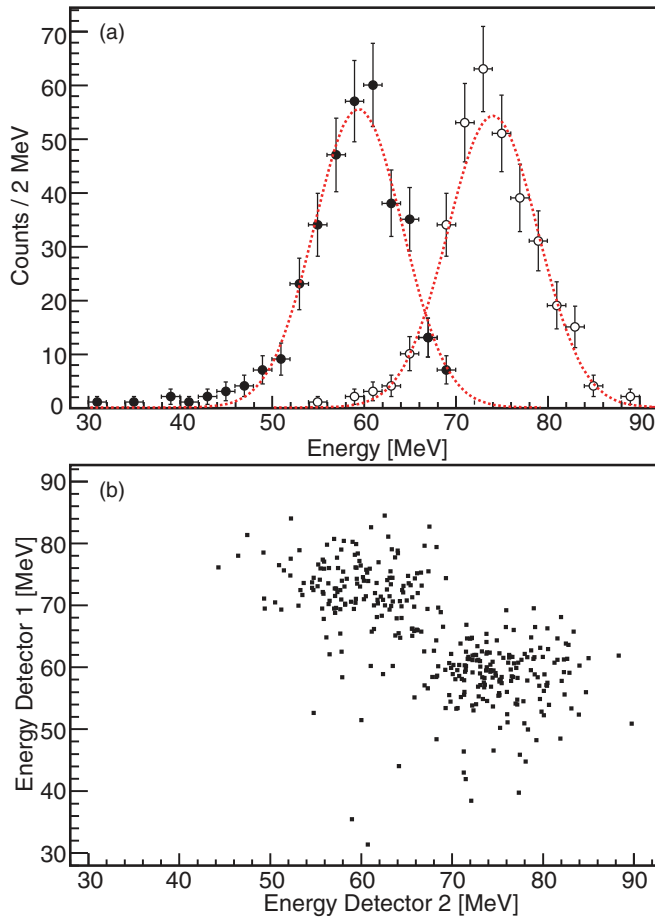
FIG. 4. (Color online) (a) Energy distribution of the fission fragments. The red dotted lines show the Gaussian fit through the data of the light and heavy fragment group. (b) Two-dimensional energy distribution of the fission fragments.

FIG. 5. (Color online) Total kinetic energy of the fission fragments. The red dotted line shows the Gaussian fit through the data.

both accidentally stable nuclei, as the most probable fission fragments of ^{180}Hg. As is discussed below, the emission of one neutron is possible in the βDF of ^{180}Tl, which would lead to ^{79}Br, ^{80}Kr, and ^{99,100}Ru as the most probable fission fragments, which are also all stable nuclei.

The fission energy distribution for 344 coincident events is shown in Fig. 4, which for the light fragment is centered around $E_L = 74.1(12)$ MeV (FWHM = 11.5(6) MeV) and for the heavy $E_H = 59.4(12)$ MeV (FWHM = 11.3(6) MeV), as deduced from a Gaussian fit through the data. The TKE spectrum, determined by summing up the energies of coincident fragments is shown in Fig. 5, which established the most probable TKE of 133.2(14) MeV with a FWHM = 15.0(9) MeV. It is interesting to note that the FWHM values obtained for the fission of ^{180}Hg are substantially smaller compared to those obtained from spontaneously fissioning nuclei in the heavy mass region (around ^{252}Cf), which are above 23 MeV [1].

The above values were deduced under the assumption of no neutrons being emitted, which was done to simplify the analysis. If neutrons are emitted, the previous results will slightly change. As neutron detectors were not employed in this experiment, no direct and precise information on the neutron emission and on the energy removed by neutrons can
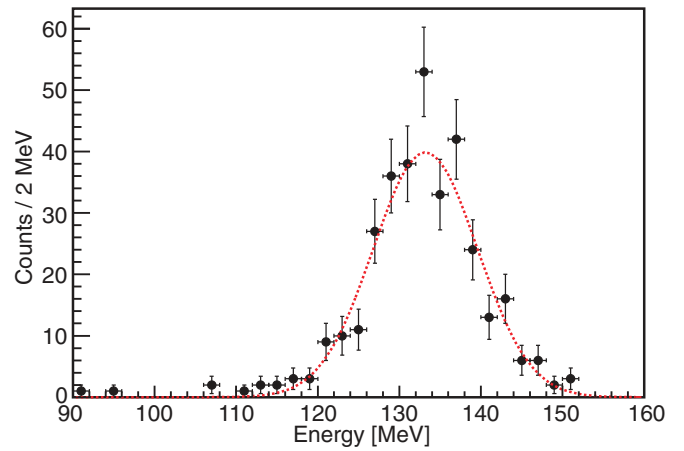
be extracted from our data. However, it is possible to infer the maximum number of neutrons that can be emitted in the fission of ^{180}Hg by comparing the calculated energy release $Q_{\mathrm{fis}}(^{180}$Hg$)$ to the deduced most probable TKE(^{180}Hg), which obviously should be smaller than the Q_{fis} value. The latter is determined as $Q_{\mathrm{fis}}(A, Z) = \Delta M(A, Z) - \Delta M(A_1, Z_1) - \Delta M(A_2, Z_2)$, where $A = A_1 + A_2$, $Z = Z_1 + Z_2$, and ΔM is the mass excess of the respective nuclei [47]. Figure 6 shows the Q_{fis} values for the most probable neutron-to-proton ratio $N/Z = 1.25$ of the light and heavy fragments as a function of the mass split fraction $M_{L,H}/180$. The three different symbols correspond to three different cases: (a) no neutron emission, (b) one-neutron emission, and (c) two-neutron emission. In particular, assuming the fragments ^{100}Ru and ^{80}Kr (thus no neutron emission), the *maximum* fission energy release is $Q_{\mathrm{fis}}(0n) = \Delta M(^{180}Hg) - \Delta M(^{100}Ru) - \Delta M(^{80}Kr) = 146.9$ MeV [47].

The maximum of the sum of the excitation energy of the two fission fragments can then be calculated as $E_{\mathrm{max,tot}}^* = Q_{\mathrm{EC}} + Q_{\mathrm{fis}}(0n) - \mathrm{TKE} = 24.5$ MeV, by using the calculated value of $Q_{\mathrm{EC}}(^{180}$Tl$) = 10.84(12)$ MeV [47]. This energy is available to be shared between the two fission fragments, γ rays and possibly emitted neutrons.

In Fig. 7 γ rays in coincidence with the fission fragments can be seen. In the spectrum one clearly observes the HgK x rays originating after the process of EC of the parent ^{180}Tl, implanted in the carbon foil. In contrast to the HgK x rays, γ rays are emitted from excited states in the fission fragments while they fly towards the silicon detectors. Therefore, these γ transitions are Doppler shifted depending on their emission angle. This explains the nonobservation of discrete γ lines, which could possibly be used to try to identify the fission fragments. The lack of statistics (only 1111 fission events were observed) and a relatively broad mass (and most probably also charge) distribution is another reason for the nonobservation of discrete γ lines. The inset of Fig. 7(b) shows the time difference between a fission fragment and a γ ray; from this can be inferred that most γ rays were detected in prompt coincidence with a fission fragment. Only 24 coincident fission-γ events were observed in the interval of 0.5–40 μs, compared to 572 events within the coincidence window of 0.5 μs. This rules
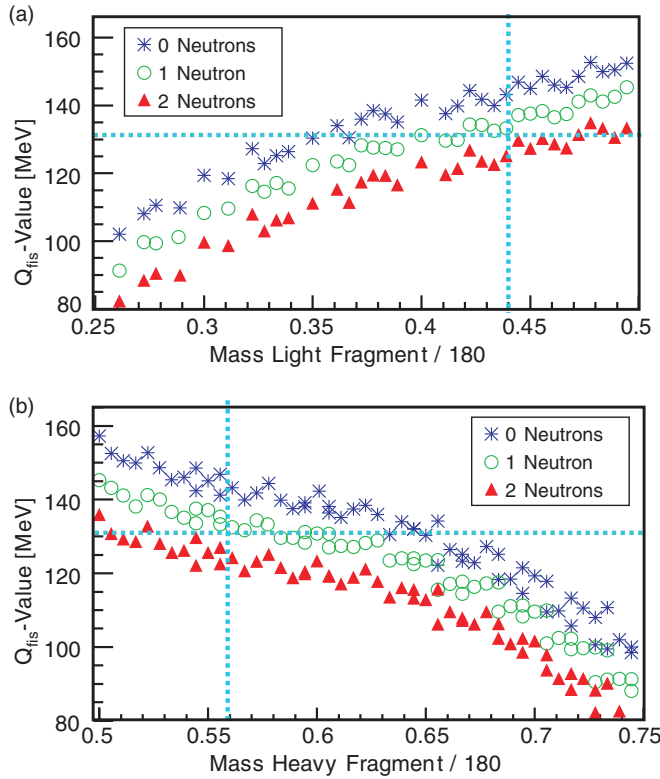
FIG. 6. (Color online) Q values for the fission of ^{180}Hg for the ratio $N/Z = 1.25(3)$ as a function of mass fraction, in (a) for the light fragment and (b) for the heavy fragment. The blue stars show the $Q_{\rm fis}$ values for the case when no neutrons are emitted, the green dots for the emission of one neutron, and the red triangles for the case of two-neutron emission. The dotted blue lines give the measured most probable total kinetic energy and the most probable mass fraction for the light and heavy fragment. The masses are taken from Ref. [47].

FIG. 7. (a) γ rays in coincidence within 0.5 μs of the detection of a fission fragment. (b) Summed γ spectrum where the energy of γ rays in coincidence with a fission fragment with a multiplicity larger than one are added up. No events were observed beyond 6.4 MeV. Data from both the Miniball cluster and the planar germanium detector were taken into account. The inset of (b) shows the time difference between between a fission fragment T_f and a γ ray T_γ.

out the γ decay from long-lived isomeric states in the fission products of ^{180}Hg.

The use of the three crystals of the Miniball (the electronic segmentation was not implemented in the current experiment) and a planar Ge detector made it possible to get an estimate of the γ multiplicity. γ rays up to a multiplicity of four were observed and the energy deposited in the Ge detectors reaches a maximum of 6.3 MeV, as can be seen in Fig. 7(b).

After accounting for the γ-ray emission, we can conclude that there is only a small chance that two neutrons can be emitted in the βDF of ^{180}Tl. This is attributable to the relatively high neutron-separation energies S_n of nuclei in the vicinity of the most probable fission fragments ^{80}Kr and ^{100}Ru. Indeed, the sum of neutron separation energies $S_n(^{80}$Kr$) = 11.521(4)$ MeV and $S_n(^{100}$Ru$) = 9.673\,32(3)$ MeV [47] gives a value close to the total available $E^* \sim 24.5$ MeV. Barely enough energy is left to account for the kinetic energy of the two neutrons and the observed γ-ray emission. We mention that based on the systematics in the uranium region, which should be sufficiently similar for the lead region, a typical mean kinetic energy of an emitted neutron in the center-of-mass system is expected to be about $\sim 0.74(2)$ MeV [53].

A similar analysis, performed for the case of a single neutron emission (see Fig. 6, green open circles), suggests
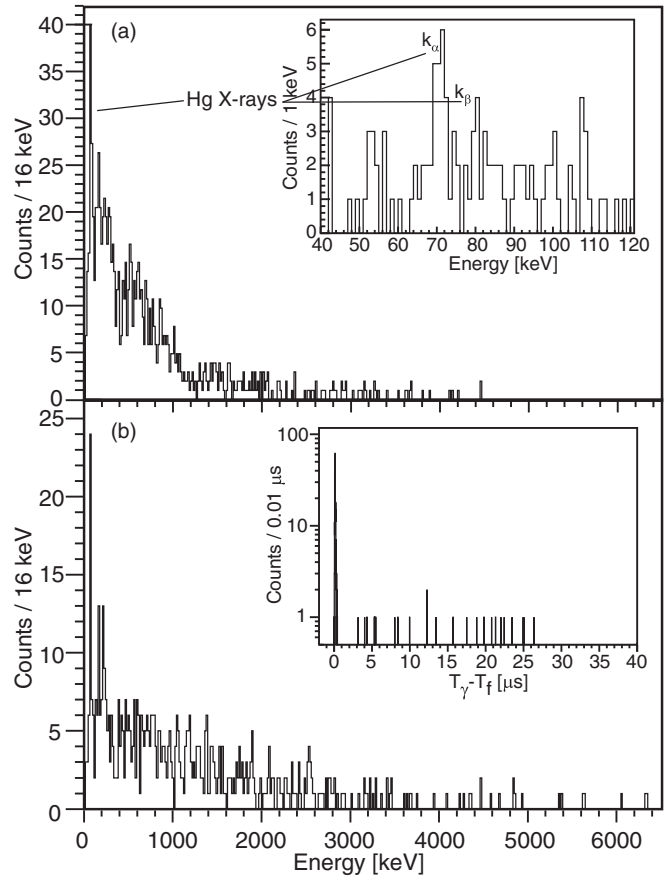
that the emission of one neutron is possible. In this case, the $Q_{\rm fis}(1n)$-value is practically exhausted by the measured most probable TKE value; thus, the total excitation energy of two fragments will be limited by the value of $Q_{\rm EC}(^{180}$Tl$) = 10.84(12)$ MeV. Owing to sharing of this energy between the two fragments, the emitted γ energy and kinetic energy of the neutron, the resulting individual excitation energies of each fragment will be below their respective S_n values. Therefore, it is hardly possible that a second neutron would be emitted, which also confirms the above analysis for the case of two-neutron emission.

Accordingly, we conclude that most probably only one neutron can be emitted in the fission of ^{180}Hg, although there is a small chance that two neutrons can be emitted. The following discussion is focused on the effect of the emission of one neutron on the mass and energy distribution. To calculate this effect, Eq. (8) has to be solved for $F_i \neq 1$. Here we assume $\nu_i = 0.5$, because the total number of emitted neutrons is one, this corresponds to 0.5 neutrons emitted by each fission fragment. Equation (8) can be solved through an iteration procedure by replacing a_i, b_i, and $\Delta E_{i,\rm cf}$ with

TABLE II. Fission properties of ^{180}Hg after β decay of ^{180}Tl. $0n$ and $1n$ denotes the case when respectively no and one neutron is emitted. All values are in MeV. Statistical uncertainties from the fit through the data are given in between brackets. Systematic uncertainties are shown in Table I.

βDF of ^{180}Tl	$0n$	$1n$
Total kinetic energy		
Most probable	133.2(14)	134.0(14)
FWHM	15.0(9)	14.3(10)
Heavy fragment energy		
Most probable	59.4(12)	59.6(12)
FWHM	11.3(6)	10.7(5)
Light fragment energy		
Most probable	74.1(12)	74.6(12)
FWHM	11.5(6)	11.3(6)

a_i/F_i, b_i/F_i, and $\Delta E_{i,\mathrm{cf}}/F_i$, respectively, in Eq. (9). The iteration process starts from the solution of Eq. (9) with $F_i = 1$, which gives the masses $m_i^\star$ when no neutrons are emitted. These can be used to calculate new factors F_i, which are used to solve Eq. (9) again, now with $F_i \neq 1$. This process is iterated until the solution obtained for $m_i^\star$ converges. This typically takes only a few iterations. By including one-neutron emission, the most probable TKE increases by about 0.8 MeV to TKE$(1n) = 134.0(14)$ MeV [FWHM $= 14.3(10)$ MeV], which is not that different from the value when no neutrons are emitted [TKE$(0n) = 133.2(14)$ MeV].

A summary of all the properties of the fragments kinetic energy distribution of the βDF of ^{180}Tl can be found in Table II.

Now we turn to the discussion of the TKE values as a function of the mass split. As mentioned earlier and shown in Fig. 3, apart from the dominant asymmetric mass split, a small contribution from symmetriclike events was also observed. The symmetric split of ^{180}Hg would be expected to lead to two semimagic spherical nuclei ^{90}Zr, for which a compact scission configuration with a high total kinetic energy should result. This situation would be similar to the so-called "high-TKE" symmetric fission mode observed in the spontaneous fission of, e.g., ^{257,258}Fm, ^{258}No, ^{259,260}Md [48,54]. These nuclei demonstrate the phenomenon of bimodal fission with two distinctive groups of events with high and low TKE values. The events in the high-TKE symmetric group have typical TKE values in the region of 230–234 MeV, which is larger by about 30 MeV than the TKE values for the "low-TKE" group. The higher TKE values are believed to occur because both fission fragments approach doubly magic spherical ^{132}Sn, which leads to a compact scission configuration. The TKE as a function of mass split for this mode demonstrates a continuous increase approaching the symmetric mass split; see, e.g., Fig. 4(a) of Ref. [48] for ^{257}Fm. In contrast, in the low-TKE mode, both fission fragments are believed to be strongly deformed, which results in an elongated scission shape with a lower TKE value. Quite often, in this mode the TKE value slightly decreases by approaching the symmetric mass split; see, e.g., Fig. 4(b) of Ref. [48] for ^{254}Cf, which points to even more strongly deformed shapes at scission.
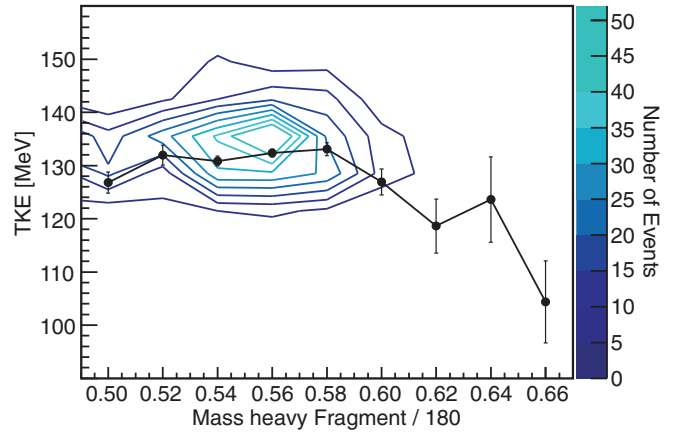

FIG. 8. (Color online) Contour diagram for the fission yield as a function of total kinetic energy and mass fraction of the heavy fragment. To draw the contours a data grouping of 7 MeV $\times$ 0.02 mass fraction units was used. The color scale gives the number of events within a contour, every contour denotes an increment of five events. The average total kinetic energy over intervals of 0.02 mass fraction units is also shown by the black dots.

A contour plot of the TKE distributions as a function of mass fraction for βDF of ^{180}Tl is shown in Fig. 8. Because only 344 coincident pairs were measured, rather coarse data grouping of 7 MeV $\times$ 0.02 mass fraction units was used, and a smoothing procedure was utilized to obtain intermediate values. The mean TKE value for each mass interval of 0.02 mass fraction units is also shown in the plot by the solid circles. Such a plot can shed more light on the specific configuration, e.g., elongation and Z_1 and Z_2, of the fragments at the scission point.

An interesting and somewhat unexpected feature of this figure is that the mean TKE for the symmetriclike fission of ^{180}Hg (mass fraction of 0.5) is about the same as the mean TKE for the observed most probable asymmetric mass split (mass fraction of $100/180 = 0.56$). As shown in Fig. 6 the Q value for symmetric mass split has the highest value; therefore, the intrinsic excitation energy TXE, being the difference of Q value and TKE, should also become maximal at the symmetric mass split. This might result in a faster washing out of the shell effects which could be present along the symmetric fission path. This might then lead to the enhanced probability of the symmetric mass split; however, no solid conclusions can be drawn here owing to the limited number of events observed at the mass-symmetric split.

Figure 9 compares the deduced most probable TKE values for ^{180}Hg with the known low-TKE data for the heavier nuclei and also with the Viola fit [55], shown by the black solid line. One can see that within the quoted experimental and systematical uncertainty the TKE(^{180}Hg) follows the systematics rather well.

B. Half-life of ^{180}Tl deduced from the βDF events

Based on the much more abundant α- and β-delayed γ decay data from the same experiment, a half-life value of $T_{1/2}(^{180}$Tl$) = 1.09(1)$ s has been determined [15,26]. Here we
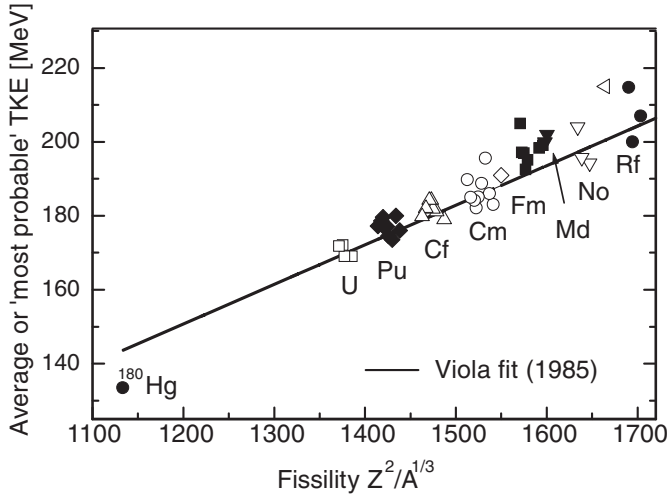
FIG. 9. A Viola plot [55], which shows the most probable TKE values for the low-TKE fission as a function of fissility for the known nuclei, together with the new value of ^{180}Hg (see text for details).

determine the $T_{1/2}$ value using the βDF branch. As mentioned in Sec. II, the proton pulses within the supercycle of 25.2 s were chosen in such a way that two consecutive (1.2 s apart) proton pulses were received, followed by a pure decay period of several seconds without protons, the whole sequence being repeated several times per supercycle (see also Fig. 2 of Ref. [26]). In the decay period, the implanted sample of ^{180}Tl decays without new implantation of thallium ions, which simplifies the half-life determination. Figure 10 shows the "decay curve" for the fission fragments resulting from the βDF of ^{180}Tl. To increase statistics, this figure was constructed by shifting in time the individual decay curves from four implantation-decay periods, corresponding to four groups of two protons within the supercycle. This decay curve was fitted by an exponential function (shown by the red dotted line) and a half-life value of $T_{1/2} = 0.94(25)$ s was deduced for the βDF of ^{180}Tl. This value is, within error bars, in agreement with the half-life determined from α and β decays [26,56].
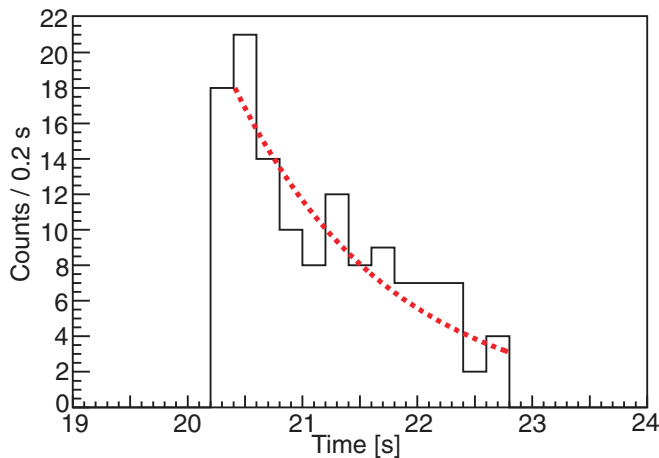

FIG. 10. (Color online) Half-life determination of ^{180}Tl through the βDF branch. The red dotted line is the exponential fit of the decay curve.

The latter fact means that both the β decay of ^{180}Tl that feeds the fissioning state in ^{180}Hg and α decay of ^{180}Tl arise from the same state in ^{180}Tl, which is most probably the $I^{\pi} = (4^-,5^-)$ ground state proposed in Ref. [26] for this nucleus. The detailed α-decay [56] and β-decay [26] studies of ^{180}Tl did not provide any evidence for an isomeric state in this nucleus.

C. βDF probability of ^{180}Tl and fission barrier of ^{180}Hg

In our original Letter on the βDF of ^{180}Tl [15], the probability for βDF $P_{\beta \mathrm{DF}}(^{180}\mathrm{Tl}) = 3.6(7) \times 10^{-3}\%$ was reported, based on 35 events which were selected for the analysis from the total amount of 344 coincident fission fragments observed. The strong reduction of the number of events was attributable to the specific selection of events used to avoid the influence of the windmill movement after each supercycle of 25.2 s on the observed number of α decays of ^{180}Hg, which is necessary for the determination of $P_{\beta \mathrm{DF}}(^{180}\mathrm{Tl})$; see discussion below. This is because, owing to the relatively long half-life of $T_{1/2}(^{180}\mathrm{Hg}) = 2.58(1)$ s, not all α decays of ^{180}Hg were measured before the activity was removed from the implantation position. This loss was especially important for the implanted ions arriving at the end of the supercycle; thus, such measurement periods were initially excluded from the analysis. We note that owing to the ~1-s half-life of ^{180}Tl and the fact that the last implantation within the supercycle happened at least 3 s before the end of the supercycle, the influence of the windmill movement on the detection of the fission events was minimal.

In the present analysis, we were able to use the single fission events measured in the silicon detector 2, thus increasing the total number of useful events to 533, which resulted in a more precise determination of the $P_{\beta \mathrm{DF}}(^{180}\mathrm{Tl})$ value. We also implemented a dedicated analysis procedure to account for the loss of α decays of ^{180}Hg owing to the windmill movement. This loss can be determined by fitting the activity of the α decays of ^{180}Hg with an exponential multigenerational decay equation. Once the parameters of this fit are determined, one can calculate the fraction of α particles that are lost by the movement of the wheel inside the windmill (details can be found in Ref. [51]). This procedure reliably calculates the loss of decays as a function of the implantation time within the supercycle.

By definition, the probability of βDF of ^{180}Tl can be determined through

$$P_{\beta \mathrm{DF}} = \frac{N_{\beta \mathrm{DF}}}{N_{\beta}(^{180}\mathrm{Tl})}$$

$$= \frac{N_{\beta \mathrm{DF}}}{N(^{180}\mathrm{Hg})} = \frac{N_{\beta \mathrm{DF}}}{2N_{\alpha}(^{180}\mathrm{Hg})/b_{\alpha}(^{180}\mathrm{Hg})}, \qquad (10)$$

in which $N_{\beta \mathrm{DF}}$ is the number of observed fission events, $N_{\beta}(^{180}\mathrm{Tl})$ is the total number of ^{180}Tl nuclei that decay through β decay, $N(^{180}\mathrm{Hg})$ and $N_{\alpha}(^{180}\mathrm{Hg})$ are the total number of daughter mercury nuclei, and the number of α decays of ^{180}Hg, respectively. As mentioned above, the number of α decays of ^{180}Hg was corrected for the effect of the windmill movement. The second equality relies on the fact that no direct production of ^{180}Hg is possible in our method, owing to the negligible probability of mercury isotopes, which are abundantly produced in the ISOLDE target, to be ionized and extracted from the target; see detailed discussion in Ref. [26].

Therefore, all ^{180}Hg observed in our spectra can originate only after the β decay of ^{180}Tl. The total number of ^{180}Hg nuclei can be determined from the observed (corrected) number of its α decay via the expression $N(^{180}\text{Hg}) = N_\alpha(^{180}\text{Hg})/b_\alpha(^{180}\text{Hg})$ [see the third equality in Eq. (10)] with the use of the known branching ratio $b_\alpha(^{180}\text{Hg}) = 48(2)\%$ [30]. The factor of 2 in the third equality stems from the fact that observing and measuring a fission fragment is twice as probable as observing an α particle. This is attributable to the fact that fission fragments are always emitted in pairs, flying in opposite directions. The resulting βDF probability is $P_{\beta\text{DF}}(^{180}\text{Tl}) = 3.2(2) \times 10^{-3}\%$.

This result is consistent, within error bars, with the less precise value of $P_{\beta\text{DF}} = 3.6(7) \times 10^{-3}\%$, which was reported in our original Letter [15].

In the work of Lazarev *et al.* [57] a value of $P_{\beta\text{DF}}(^{180}\text{Tl}) = 3 \times 10^{-(5\pm1)}\%$ was reported. It was deduced from the ratio of the measured fission cross section and estimated production cross section of $\sigma(^{180}\text{Tl}) \sim 0.1$–1 mb in the reaction $^{40}\text{Ca} + ^{144}\text{Sm} \rightarrow {}^{180}\text{Tl} + p3n$; see also Ref. [14]. The latter rough estimate was made by the authors of Ref. [14] based on the statistical model code.

To test the correctness of this value, we performed our own statistical model calculations of the expected production cross section of ^{180}Tl in the $^{40}\text{Ca} + ^{144}\text{Sm} \rightarrow {}^{180}\text{Tl} + p3n$ reaction. Calculations were based on the analysis of the production cross section data recently obtained in the Pb-Po region of nuclei with a large set of similar complete-fusion reactions with heavy ions; see, e.g., Ref. [58] and references therein. The obtained $\sigma(^{180}\text{Tl})$ was in the range of several μb, which is $\sim$100–1000 times lower than the value estimated in Ref. [14]. If one now uses our cross-section estimate instead of 0.1–1 mb, used by Lazarev *et al.*, the $P_{\beta\text{DF}}(^{180}\text{Tl})$ value from Ref. [57] will increase by the corresponding factor and will become comparable, within the uncertainties, with our value from the ISOLDE experiment.

The deduced $P_{\beta\text{DF}}(^{180}\text{Tl})$ value can be used to estimate the value of the fission barrier height B_f for ^{180}Hg. For this procedure, the knowledge (experimental or theoretical) of several parameters is required, the most important being the $Q_{\text{EC}}(^{180}\text{Tl})$, the β-decay strength function $S_\beta(^{180}\text{Tl})$, the level density, and the Γ_γ width for ^{180}Hg. Though admittedly somewhat model-dependent, this approach was applied in several earlier βDF studies in the transuranium and lead regions; see, e.g., Ref. [59–62].

By using this framework, and employing several sets of input parameters to check the consistency of the analysis, the fission barrier of ^{180}Hg was estimated to be in the range of 6.76–8.96 MeV; see detailed discussion in our complementary work [62]. Despite the broad range, all values are consistently lower than all theoretical fission barriers which lie in the range of 9.69–11.40 MeV. This confirms the well-known discrepancy between the experimentally deduced and calculated fission barriers for the extremely neutron-deficient nuclei [62].

D. Recent theoretical studies of the fission of mercury isotopes

In our first paper on βDF of ^{180}Tl, the five-dimensional fission model [63] was used to explain the observed

asymmetric mass split of fission fragments. Recently, fission fragment mass yield calculations for a long chain of even-A $^{174-188}$Hg isotopes were performed [20] using the Brownian Metropolis shape-motion treatment [64]. Both types of calculations are in agreement with each other and show asymmetric mass distributions with only a small contribution from a symmetric mass split. An interesting inference of the latter work was the prediction that the mass asymmetry will be preserved at higher excitation energies, at least up to $E^* = 40$ MeV; see Fig. 6 of Ref. [20]. It would be very important to check these predictions in the future experiments by using, e.g., fusion-fission reactions with heavy ions.

Furthermore, in Ref. [65], the authors calculated and analyzed five-dimensional potential-energy surfaces of 12 even $^{178-200}$Hg isotopes in the very neutron-deficient region. The most important finding in this work is that it is only for nuclei in the range $180 < A < 190$ that the saddle region is somewhat shielded from the symmetric fusion valley by a moderately high ridge that also has some moderate extension in the elongation direction.

Another recent theoretical study of the fission of mercury isotopes was performed in Ref. [21]. The authors used the self-consistent nuclear density functional theory employing Skyrme and Gogny energy density functionals. The potential energy surfaces in multidimensional space of collective coordinates, including elongation, triaxiality, reflection asymmetry, and necking, were calculated for ^{180}Hg and ^{198}Hg. The asymmetric fission valleys, well separated from fusion valleys associated with nearly spherical fragments, were found in both cases. Moreover, these calculations suggest ^{100}Ru/^{80}Kr as most probably mass split, consistent with our experimental findings.

In a different approach, by using what the authors call an "improved scission-point" model [23], the mass distributions were calculated for induced fission of $^{180-196}$Hg isotopes. The asymmetric mass distribution of fission fragments of ^{180}Hg was also demonstrated, with the calculated mass distribution and mean total kinetic energy of fission fragments being in good agreement with the available experimental data. The drastic change in the shape of the mass distribution from asymmetric to symmetric was predicted with increasing mass number of the fissioning mercury isotope.

Finally, the authors of Ref. [24] used the recently developed microscopic scission-point model. This model goes far beyond the liquid drop description used in the original model of Wilkins *et al.* [22]. By using this model, the asymmetric fission mass distribution for ^{180}Hg at low energy could be described on the sole basis of the fragment structure and deformed shell effects.

Thus, it appears that the conclusion on the asymmetric mass split of ^{180}Hg is a robust one also from the theoretical point of view and is well reproduced by different modern theoretical approaches.

V. CONCLUSION

In the βDF of ^{180}Tl a symmetric mass distribution centered around the semi-doubly-magic nucleus ^{90}Zr, was expected in the fission of the daughter nucleus ^{180}Hg. Instead, it was

observed that ^{180}Hg fissions in two fragments of unequal mass centered around mass number $A = 80$ and 100. The most probable fission fragments were determined to be ^{100}Ru and ^{80}Kr. Based on the energy balance, most probably only one neutron could be emitted.

The TKE for the different mass splits was compared and has, within error bars, the same most probable value for all observed fission fragment pairs.

In addition to the above-mentioned results, in the present work a βDF probability of $P_{\beta DF}(^{180}$Tl$) = 3.2(2) \times 10^{-3}$% was determined.

Several recent successful experiments conducted at ISOLDE-CERN searching for a βDF branch in other isotopes in the neutron-deficient lead region will shed more light on low-energy fission in this part of the nuclear chart.

[1] C. Wagemans, *The Nuclear Fission Process* (CRC Press, Boca Raton, FL, 1991), and references therein.

[2] H. L. Hall *et al.*, J. Radiol. Nucl. Chem. **142**, 53 (1990).

[3] R. Vandenbosch, Annu. Rev. Nucl. Part. Sci. **27**, 1 (1977).

[4] A. Bail *et al.*, Phys. Rev. C **84**, 034605 (2011), and references therein.

[5] K.-H. Schmidt *et al.*, Nucl. Phys. A **693**, 169 (2001).

[6] K.-H. Schmidt *et al.*, Nucl. Phys. A **665**, 221 (2000).

[7] V. I. Kuznetsov and N. K. Skobelev, Yad. Fiz. **4**, 279 (1966).

[8] H. L. Hall and D. C. Hoffman, Annu. Rev. Nucl. Part. Sci. **42**, 147 (1992).

[9] M. G. Itkis *et al.*, Sov. J. Nucl. Phys. **52**, 601 (1990).

[10] M. G. Itkis *et al.*, Sov. J. Nucl. Phys. **53**, 757 (1991).

[11] D. A. Shaughnessy *et al.*, Phys. Rev. C **61**, 044609 (2000).

[12] D. A. Shaughnessy *et al.*, Phys. Rev. C **65**, 024612 (2002).

[13] S. A. Kreek *et al.*, Phys. Rev. C **49**, 1859 (1994).

[14] Y. A. Lazarev *et al.*, Europhys. Lett. **4**, 893 (1987).

[15] A. N. Andreyev *et al.*, Phys. Rev. Lett. **105**, 252502 (2010).

[16] A. N. Andreyev *et al.*, Phys. Rev. C **87**, 014317 (2013).

[17] J. F. W. Lane *et al.*, Phys. Rev. C **87**, 014318 (2013).

[18] A. N. Andreyev, M. Huyse, and P. Van Duppen, Rev. Mod. Phys. **85**, 1541 (2013).

[19] P. Moller, A. J. Sierk, T. Ichikawa, A. Iwamoto, R. Bengtsson, H. Uhrenholt, and S. Aberg, Phys. Rev. C **79**, 064304 (2009).

[20] P. Möller, J. Randrup, and A. J. Sierk, Phys. Rev. C **85**, 024306 (2012).

[21] M. Warda, A. Staszczak, and W. Nazarewicz, Phys. Rev. C **86**, 024601 (2012).

[22] B. D. Wilkins *et al.*, Phys. Rev. C **14**, 1832 (1976).

[23] A. V. Andreev, G. G. Adamian, and N. V. Antonenko, Phys. Rev. C **86**, 044315 (2012).

[24] S. Panebianco, J. L. Sida, H. Goutte, J. F. Lemaitre, N. Dubray, and S. Hilaire, Phys. Rev. C **86**, 064601 (2012).

[25] E. Kugler, Hyperfine Interact. **129**, 23 (2000).

[26] J. Elseviers *et al.*, Phys. Rev. C **84**, 034307 (2011).

[27] V. Liberati *et al.*, preceding paper, Phys. Rev. C **88**, 044322 (2013).

[28] V. N. Fedosseev *et al.*, Rev. Sci. Instrum. **83**, 02A903 (2012).

[29] T. J. Giles *et al.*, Nucl. Instrum. Methods Phys. Res., Sect. B **204**, 497 (2003).

[30] ENSDF-Evaluated Nuclear Structure Data File, http://www.nndc.bnl.gov/ensdf/

[31] Ortec, http://www.ortec-online.com.

[32] Canberra, http://www.canberra.com.

[33] S. Agostinelli *et al.*, Nucl. Instrum. Methods Phys. Res., Sect. A **506**, 250 (2003).

[34] J. Eberth *et al.*, Progr. Part. Nucl. Phys. **46**, 389 (2001).

[35] P. Van Duppen *et al.*, Nucl. Instrum. Methods Phys. Res., Sect. A **254**, 401 (1987).

[36] X-ray Instruments Associates, http://www.xia.com.

[37] H. W. Schmitt *et al.*, Phys. Rev. **137**, B837 (1965).

[38] E. Weissenberger *et al.*, Nucl. Instrum. Methods Phys. Res., Sect. A **248**, 506 (1986).

[39] E. P. Steinberg *et al.*, Nucl. Instrum. Methods **99**, 309 (1972).

[40] E. C. Finch *et al.*, Nucl. Instrum. Methods **113**, 29 (1973).

[41] L. Ghys *et al.* (private communication).

[42] E. C. Finch *et al.*, Nucl. Instrum. Methods **142**, 539 (1977).

[43] M. Ogihara *et al.*, Nucl. Instrum. Methods Phys. Res., Sect. A **251**, 313 (1986).

[44] A. Menchaca-Rocha *et al.*, Nucl. Instrum. Methods Phys. Res., Sect. B **207**, 356 (2003).

[45] Janis 3, http://www.oecd-nea.org/janis/

[46] H. W. Schmitt *et al.*, Phys. Rev. **141**, 1146 (1966).

[47] G. Audi *et al.*, Nucl. Phys. A **729**, 337 (2003).

[48] J. P. Balagna *et al.*, Phys. Rev. Lett. **26**, 145 (1971).

[49] D. C. Hoffman *et al.*, Phys. Rev. C **41**, 631 (1990).

[50] SRIM-The Stopping and Range of Ions in Matter, http://www.srim.org/

[51] J. Elseviers, Master's thesis, University of Leuven, Faculteit Wetenschappen, 2009.

[52] S. Sels, Master's thesis, University of Leuven, Faculteit Wetenschappen, 2013.

[53] J. Terrel, Phys. Rev. **127**, 880 (1962).

[54] E. K. Hulet *et al.*, Phys. Rev. C **40**, 770 (1989).

[55] V. E. Viola, K. Kwiatkowski, and M. Walker, Phys. Rev. C **31**, 1550 (1985).

[56] A. N. Andreyev (private communication).

[57] Y. A. Lazarev *et al.*, Inst. Phys. Conf. Ser. **N132**, 739 (1992).

[58] A. N. Andreyev *et al.*, Phys. Rev. C **72**, 014612 (2005).

[59] D. Habs *et al.*, Z. Phys. A **285**, 53 (1978).

[60] A. Staudt, M. Hirsch, K. Muto, and H. V. Klapdor-Kleingrothaus, Phys. Rev. Lett. **65**, 1543 (1990).

[61] A. N. Andreyev *et al*., Phys. Lett. B **312**, 49 (1993).

[62] M. Veselský *et al*., Phys. Rev. C **86**, 024308 (2012).

[63] P. Möller *et al*., Nature (London) **409**, 785 (2001).

[64] J. Randrup and P. Möller, Phys. Rev. Lett. **106**, 132503 (2011).

[65] T. Ichikawa, A. Iwamoto, P. Möller, and A. J. Sierk, Phys. Rev. C **86**, 024610 (2012).